Applied Catalysis B: Environmental 180 (2016) 78–85

Contents lists available at ScienceDirect

Applied Catalysis B: Environmental

journal homepage: www.elsevier.com/locate/apcatb

# Carbon supported $Pt_9Sn_1$ nanoparticles as an efficient nanocatalyst for glycerol oxidation

Jian Dou[a], Bowei Zhang[b], Hai Liu[b], Jindui Hong[a], Shengming Yin[a], Yizhong Huang[b,*], Rong Xu[a,*]

[a] School of Chemical & Biomedical Engineering, Nanyang Technological University, 62 Nanyang Drive, 637459, Singapore
[b] School of Materials Science and Engineering, Nanyang Technological University, 50 Nanyang Avenue, 639798, Singapore

ARTICLE INFO

*Article history:*
Received 28 March 2015
Received in revised form 3 June 2015
Accepted 4 June 2015
Available online 6 June 2015

*Keywords:*
Nanocatalyst
Stannous oxide
Platinum
Glycerol
Oxidation

ABSTRACT

Glycerol derived from biomass is increasingly attractive as a renewable feedstock for production of bulk and specialty chemicals. In this work, we have developed an efficient $Pt_9Sn_1$/C nanocatalyst for oxidation of glycerol to glyceric acid, with its activity the highest among various PtM/C (M = Mn, Fe, Co, Ni, Cu, Zn, Au) bimetallic nanocatalysts. Under the optimized conditions, 91% of glycerol can be oxidized within 8 h at 60 °C, with 50% yield of glyceric acid. Without incorporation of Sn, a lower glycerol conversion of around 69% was obtained over the monometallic 2.0%Pt/C-R catalyst under the same reaction conditions. Furthermore, the calculated turn over frequency (TOF) based on surface Pt atoms is 938 $h^{-1}$ for 2.0%$Pt_9Sn_1$/C-R nanocatalyst, which is three times as high as that of 2.0%Pt/C-R catalyst (281 $h^{-1}$). The enhancement of activity by modifying Pt nanoparticles with Sn is attributed to activation of oxygen molecules and/or deprotonation of hydroxyl group by surface stannous oxide (SnO) species. In addition, the $Pt_9Sn_1$/C-R catalyst has been shown to be robust and stable without substantial loss of activity after being recycled for four times.



## 1. Introduction

Glycerol, as a side product from biodiesel production, has been identified as a key platform chemical for producing valuable chemicals [1,2]. Conversion of glycerol via different reaction pathways such as oxidation, hydrogenolysis, and dehydration etc. has been investigated extensively over the last decade [3,4]. Particularly, processes such as chlorination of glycerol to epichlorohydrin, esterification of glycerol to glycerol acetates, and steam reforming of glycerol to syngas have been practiced in industry [2]. Other than bulk chemicals, it is also desirable to produce high value fine chemicals from glycerol. For example, oxidation of glycerol generates various oxygenated products such as glyceric acid, dihydroxyacetone, hydroxypyruvic acid, and glycolic acid etc., which find potential applications in polymer and fine chemical industries [3].

Generally, heterogeneous noble metal catalysts (i.e., Pt, Pd, and Au based catalysts) coupled with green oxidants such as oxygen are considered as a more sustainable system for glycerol oxidation [5–12]. For instance, activated carbon supported Pt catalyst (5%Pt/C) was reported to be very active for glycerol oxidation, with 55% yield of glyceric acid at 90% conversion (pH was adjusted to 7 by adding 30% NaOH solution). With 5%Pd/C catalyst, the yield of glyceric acid was increased to 70% under the basic condition (pH 11) [13]. A high yield of 83% glyceric acid was achieved over 1%Au/C catalyst in 0.6 M NaOH solution [14]. Generally, sodium hydroxide was used along with noble metal catalysts for glycerol oxidation. Without adding a base, gold based catalysts were found totally inactive for oxidation of glycerol [11]. The role of base is to activate glycerol molecules by deprotonation of hydroxyl group, which is one of the rate limiting steps [15,16]. However, the products formed are salts instead of acids with the addition of the base in the reaction mixture, which requires further neutralization steps and generates inorganic salt waste. Thus many research efforts have been devoted to developing efficient noble metal based catalysts for glycerol oxidation under base free conditions [17–20]. Recently, various supported gold catalysts have been used for glycol oxidation under base free condition using $H_2O_2$ as the oxidant [21].

In order to prepare efficient catalysts for base free glycerol oxidation, basic catalyst supports such as magnesium oxide (MgO) and magnesium enriched layered double hydroxide have been used for deposition of Pt and Pt based nanoparticles [22–24]. For example, magnesium oxide supported PtAu catalysts showed promising

* Corresponding authors.
*E-mail addresses:* YZHUANG@ntu.edu.sg (Y. Huang), RXu@ntu.edu.sg (R. Xu).

http://dx.doi.org/10.1016/j.apcatb.2015.06.007
0926-3373/

activities for glyceric acid production from glycerol. At 60 °C, 30.9% yield of glyceric acid was achieved at 42.9% of conversion of glycerol. The calculated turnover frequency (TOF, defined as moles of glycerol converted per mole of total Pt loading per hour) was 107 $h^{-1}$ [24]. As glyceric acid is one of the reaction products, the pH of the reaction mixture can reach around 2 to 3, which poses the question on the long term stability of the basic supports. Among the noble metals investigated so far, Pt is the most active catalyst for glycerol oxidation [20]. By alloying metals with Pt, the selectivity of oxidation products can be finely tuned. For example, the selectivity of glyceric acid was higher with PtAu catalyst (79%) than that with Pt alone catalyst (45%), while the conversion of glycerol decreased from 78 to 45% at reaction time of 2 h [20]. With PtBi, PtSb and PdAg catalysts, the major oxidation product was switched from glyceric acid to dihydroxyacetone [25–27]. It remains challenging to prepare Pt based nanocatalysts on non-basic catalyst supports with high activity and high selectivity for glyceric acid production from glycerol.

In this work, a range of Pt based bimetallic nanocatalysts were prepared and investigated for glycerol oxidation. Among the various Pt based bimetallic nanocatalysts, PtSn nanoparticle supported on activated carbon has been demonstrated to be the most active catalyst for glyceric acid production from glycerol. The synthesis parameters, loading of PtSn nanoparticles, and activation conditions were systematically varied to generate the most efficient catalyst. The prepared nanocatalysts were extensively characterized to understand the active sites of the PtSn/C-R nanocatalyst. In addition, the stability of the PtSn nanocatalysts was studied by recycle test.

## 2. Experimental

### 2.1. Preparation of PtM (M = Sn, Mn, Fe, Cu, Ni, Cu, Zn, Au) bimetallic nanoparticles

PtM bimetallic nanoparticles were prepared following the literature method with slight modification [28–30]. Briefly, 40 mg of sodium hydroxide (NaOH, 98+%, Sigma–Aldrich) was dissolved in 8.67 mL of ethylene glycol (EG, $C_2H_6O_2$, 99%, Alfa Aesar), followed by adding 1.00 mL of 0.05 M ethylene glycol solution of chloroplatinic acid ($H_2PtCl_6{\cdot}xH_2O$, 99.9+%, Sigma–Aldrich) and 0.33 mL of 0.05 M ethylene glycol solution of tin (II) chloride ($SnCl_2{\cdot}2H_2O$, 98%, Sigma–Aldrich). The resulted solution was heated to 160 °C and refluxed for 3 h. Other PtM bimetallic nanoparticles were prepared similarly using the above-mentioned procedures. PtSn nanoparticles with different Pt/Sn ratios were prepared by adjusting the $H_2PtCl_6{\cdot}xH_2O$/ $SnCl_2{\cdot}2H_2O$ ratio in the range of 1:1–20:1.

### 2.2. Deposition of PtM bimetallic nanoparticles onto activated carbon support

The as-synthesized PtM bimetallic nanoparticles were immobilized onto activated carbon support via colloid deposition method to obtain 0.5–2% of Pt loading. For example, 3 mL of as-prepared $Pt_9Sn_1$ colloid suspension was added to 300 mg of activated carbon (Sigma–Aldrich, specific surface area = 1500 $m^2$/g). The resultant mixture was stirred at room temperature for 3 h. The solid sample was then collected by filtration and washed with deionized water. The solid product was dried at 60 °C overnight, and was denoted as $Pt_9Sn_1$/C. The prepared samples were further reduced at 300 °C for 3 h with 30 mL/min of $H_2$. The reduced samples were denoted as $Pt_9Sn_1$/C-R. Other PtM bimetallic nanoparticles were deposited onto activated carbon support similarly.

### 2.3. Oxidation of glycerol

The liquid phase oxidation of glycerol was carried out in a 50 mL 3-necked round bottom flask coupled with a reflux condenser in a temperature controlled oil bath. In a typical reaction, 50 mg of catalyst was added to 10 mL of 0.5 M glycerol ($C_3H_8O_3$, 99+%, Alfa Aesar) aqueous solution. The reaction was carried out at 60 °C for 2–10 h with purified oxygen bubbling through at 15 mL/min. The liquid products were analyzed with high performance liquid chromatography (HPLC, Agilent) coupled with ultraviolet (UV) and refractive index (RI) detectors. The liquid analytes were separated using an Alltech OA-1000 organic acid column (300 mm × 6.5 mm, ID = 9 μm), eluted with 4 mM $H_2SO_4$ aqueous solution at 80 °C. External standards were used to quantify the reaction products. The stability of the optimized nanocatalyst was tested by recycling for 4 runs. After each run, the reaction mixture was filtered and the catalyst was washed with deionized water. The spent catalyst was dried at 60 °C overnight followed by reduction at 400 °C in hydrogen atmosphere before the next run.

### 2.4. Materials characterization

The crystallographic structure of the solid samples was investigated using powder X-ray diffraction (XRD, Bruker D2, CuKα, λ = 1.5406 Å). The morphology and chemical composition of the solid samples were examined with transmission electron microscopy (TEM, JEM3010, 300 kV), high resolution transmission electron microscopy (HRTEM, JEM2100, 200 kV) and energy dispersive X-ray spectroscopy (EDX, Oxford). The chemical states of Pt and Sn were analyzed with X-ray photoelectron spectroscopy (XPS, VG ESCALAB 220I-XL) using a monochromatized Al Kα exciting radiation (1486.71 eV), and all binding energies (BE) were referenced to the C 1s peak (BE = 284.5 eV). The loading of Pt and Sn was measured by inductively coupled plasma optical emission spectroscopy (ICP-OES, Perkin Elmer ICP Optima 2000 V). Chemisorption uptakes of CO were measured using static volumetric methods (Micromeritics ASAP 2020 analyzer). In a typical run, around 100 mg of sample was firstly reduced at 400 °C for 2 h (heating rate 10 °C/min) in $H_2$ flow (20 mL/min). After that, the sample was cooled to 35 °C under He flow (20 mL/min). An initial isotherm was measured at 35 °C in an adsorbate (CO) pressure range of 60–600 mmHg. Next, reversibly adsorbed CO molecules were removed by evacuation at 35 °C for 30 min before measuring a repetitive isotherm under the same conditions as the initial one. The difference between the initial and repetitive isotherm reflected the uptake of irreversibly chemisorbed CO on catalysts. CO uptake was determined by the mean value of five points in the pressure range of 300–500 mmHg of the difference isotherm.

## 3. Results and discussion

### 3.1. Catalyst properties

Platinum based bimetallic nanoparticles were prepared by ethylene glycol assisted reduction method in alkaline solution. It is noted that ethylene glycol assisted reduction method has been used to prepare noble metal nanoparticles such as Pt, Ru, Rh with sizes of 1–3 nm [30]. Later this method has been extended to prepare Pt based bimetallic nanoparticles such as PtRu and PtSn nanoparticles [29,31]. For example, $Pt_3Sn_1$ nanoparticles have been prepared by reduction of Pt and Sn precursors in alkaline solution in ethylene glycol along with a minor percentage of tin dioxide ($SnO_2$) precipiated [28,29]. Since tin dioxide can be dissolved in alkaline solution, it was anticipated that the minor amount of tin dioxide can be removed by presence of sodium hydroxide. In the present work,

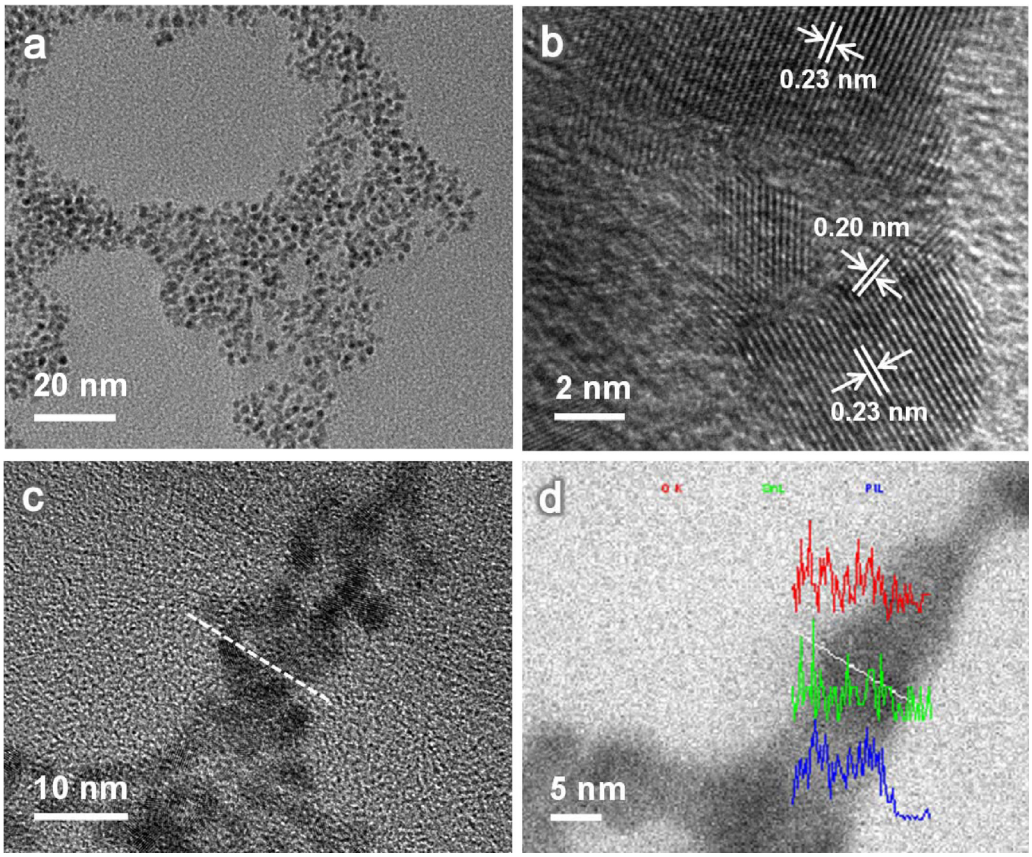


**Fig. 1.** (a) TEM and (b) HRTEM images of as-synthesized $Pt_9Sn_1$ nanoparticles; (c) HRTEM and (d) STEM-EDX line scan on $Pt_9Sn_1$ nanoparticles at the same location. The blue, green, and red lines represent signals from Pt, Sn, and O elements respectively. (For interpretation of the references to color in this figure legend, the reader is referred to the web version of this article.)

sodium hydroxide solution in ethylene glycol with a concentration of 0.1 M was used to prepare PtSn nanoparticles. As shown in Fig. 1a and S1, $Pt_9Sn_1$ nanoparticles with sizes of 1–3 nm were successfully prepared. Based on the HRTEM image (Fig. 1b), the lattice space of 0.23 nm and 0.20 nm can be assigned to (1 1 1) and (2 0 0) planes of cubic Pt metal, respectively (JCPDS 04-0802). The presence of Sn in the prepared $Pt_9Sn_1$ bimetallic nanoparticles is evidenced by EDX line scan of the two neighbouring nanoparticles (Fig. 1c). As shown in Fig. 1d, two peaks can be observed from Pt (blue) and O (red) lines, correlating well with HRTEM images in Fig. 1c. The two peaks from Sn line (green) are less intense comparing to those in Pt and O lines, suggesting a relatively low concentration of Sn element in the $Pt_9Sn_1$ nanoparticles. EDX line scan was also carried out on assembly of $Pt_9Sn_1$ nanoparticles (Fig. S2). As shown in Fig. S2, the peak for Sn element (in green line) is clearly observed, further confirming the existence of Sn in the $Pt_9Sn_1$ bimetallic nanoparticles.

The freshly prepared $Pt_9Sn_1$ nanoparticles were immobilized onto carbon support via colloid deposition method followed by reduction in hydrogen. The loading of Pt in the final catalyst is varied from 0.5 to 2.0%. The carbon supported $Pt_9Sn_1$ nanocatalyst was characterized by XRD. As shown in Fig. 2, the activated carbon support has several peaks at 36.7, 39.6, and 42.5° (JCPDS 46-0944). For supported Pt nanoparticles (2%Pt/C-R), two peaks can be found at 39.9 and 46.4°, attributed to (1 1 1) and (2 0 0) peaks of metallic Pt with a cubic phase (JCPDS 04-0802). It can be noted that the (1 1 1) peak overlaps with the peak from carbon support. The XRD patterns of as-synthesized and reduced carbon supported $Pt_9Sn_1$ nanocatalysts (2.0%$Pt_9Sn_1$/C and 2.0%$Pt_9Sn_1$-R) are similar. Two peaks are observed at 39.7 and 46.1°, corresponding to the (1 1 1) and (2 0 0) peaks of cubic Pt metal, respectively. It is noted that these two peaks

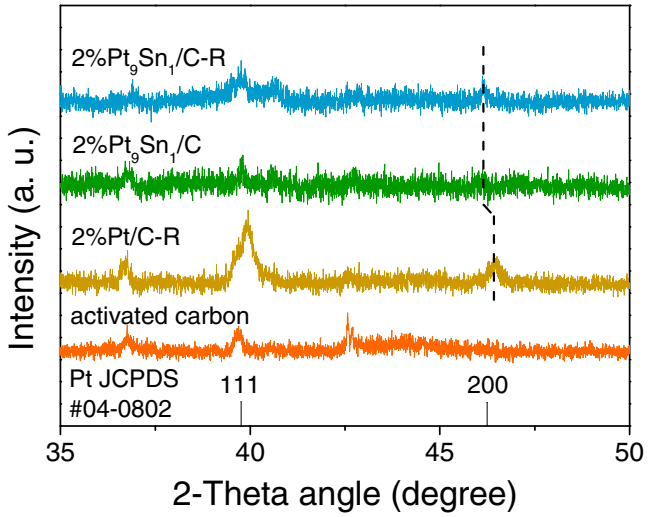


**Fig. 2.** XRD patterns of carbon support, 2%Pt/C-R, 2%$Pt_9Sn_1$/C and 2%$Pt_9Sn_1$/C-R nanocatalysts.

are shifted to lower angles compared to those of Pt/C-R catalyst, suggesting the formation of PtSn alloys [28,29]. Nevertheless, due to a low percentage of metals in the sample and very small particle sizes, it is difficult to determine the exact state and location of Sn in PtSn the nanoparticles. There are no peaks belonging to SnO or $SnO_2$ observed. The XRD pattern of 0.5%$Pt_9Sn_1$/C-R is similar to that of 2.0%$Pt_9Sn_1$/C-R nanocatalyst (Fig. S3).

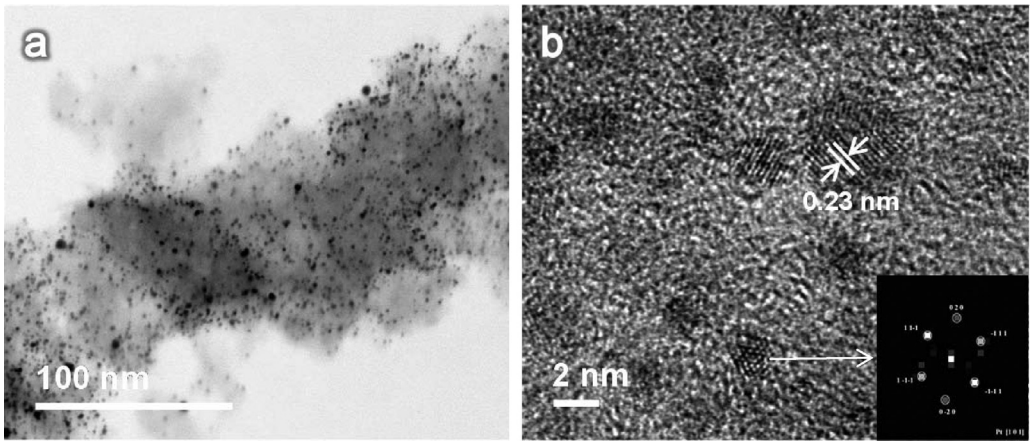


**Fig. 3.** (a) STEM and (b) HRTEM images of supported 2%$Pt_9Sn_1$/C-R nanocatalyst. Inset shows the FFT pattern of one $Pt_9Sn_1$ particle in (b).

As displayed in Fig. S4, $Pt_9Sn_1$ nanoparticles with size of 1–3 nm are well dispersed on the surface of activated carbon for 0.5%$Pt_9Sn_1$/C-R nanocatalyst. The lattice spacing of 0.23 nm is attributed to (1 1 1) plane of Pt metal with a cubic phase, as mentioned above. By increasing the loading of Pt to 2.0%, there is no significant aggregation of $Pt_9Sn_1$ nanoparticles as observed for 2.0%$Pt_9Sn_1$/C-R nanocatalyst (Fig. 3a and S5). The dispersion of $Pt_9Sn_1$ nanoparticles on 2.0%$Pt_9Sn_1$/C-R sample is similar as that on 0.5%$Pt_9Sn_1$/C-R nanocatalyst, suggesting the colloid immobilization method is effective for preparation of nanocatalysts with well dispersed active components. Similarly, the observed lattice spacing of 0.23 nm is attributed to (1 1 1) plane of Pt metal (Fig. 3b), which has also been confirmed by FFT pattern shown in the inset.

The oxidation states of various elements in 2.0%$Pt_9Sn_1$/C-R nanocatalysts were characterized by XPS technique. All the binding energies were referenced to 284.5 eV arising from C—C bond. The XPS spectra for reduced 2.0%$Pt_9Sn_1$/C-R sample are presented in Fig. 4. In Fig. 4a, the peak at 284.5 eV is attributed to surface C—C bonds. The peak at 285.8 eV could be assigned to carbon atoms attached to surface hydroxyl or C=O=C group, and the third peak at 286.8 eV is attributed to surface C=O moiety [32]. The Pt $4f_{5/2}$ peak could be deconvoluted into two peaks at 71.5 and 72.6 eV (Fig. 4b). These two peaks are attributed to $Pt^0$ and $Pt^{2+}$ respectively, which could be possibly due to partial oxidation of the surface Pt atoms [33,34]. The incorporation of Sn element in the 2.0%$Pt_9Sn_1$/C-R nanocatalyst was further confirmed by the XPS spectrum of Sn (Fig. 4c). The Sn $3d_{3/2}$ peak at 486.4 eV could be assigned to $Sn^{2+}$,

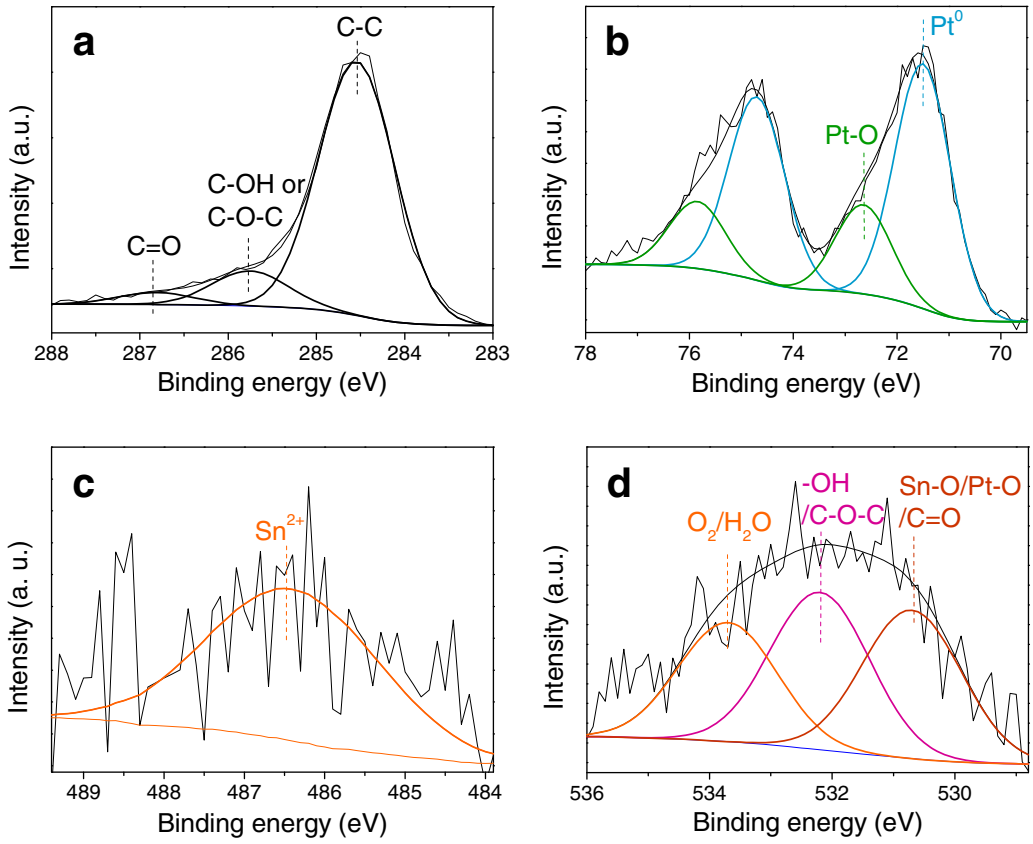


**Fig. 4.** XPS spectra of (a) C 1s, (b) Pt 4f, (c) Sn 3d, and (d) O 1s of 2%$Pt_9Sn_1$/C-R nanocatalyst.

**Table 1**
Physical properties of 2%$Pt_9Sn_1$/C-R, 2%$Pt_{0.8}Sn_1$/C-R, and 2%Pt/C-R nanocatalysts.

| Catalyst | Loading (wt%)[a] | | CO chemisorption (μmol/g)[b] | Dispersion (%)[b] | Size (nm)[c] |
|---|---|---|---|---|---|
| | Pt | Sn | | | |
| 2%Pt/C-R | 1.8 | – | 48.9 | 52.9 | 1.6 ± 0.6 |
| 2%$Pt_9Sn_1$/C-R | 2.0 | 0.2 | 23.5 | 22.9 | 1.8 ± 0.6 |
| 2%$Pt_{0.8}Sn_1$/C-R | 1.8 | 0.5 | 0.7 | 0.7 | 3.2 ± 1.2 |

[a] Determined by ICP analysis.
[b] Determined by CO chemisorption.
[c] Measured from TEM images.

suggesting that the Sn element in $Pt_9Sn_1$ nanoparticles is partially oxidized [33]. It was reported that Sn mainly exists in oxidized state in PtSn alloy nanoparticles [28,29]. The O 1s spectrum was deconvoluted to three peaks centered at 530.7, 532.2 and 533.7 eV, corresponding to oxygen in SnO/PtO and/or carbonyl group, surface hydroxyl and/or ether group, and surface adsorbed oxygen and/or water respectively. The content of Pt and Sn in the supported 2.0%$Pt_9Sn_1$/C nanocatalyst was estimated from the peak area of Pt and Sn, corrected by their sensitivity factors. The surface Pt/Sn ratio calculated from XPS results is around 9 in 2.0%$Pt_9Sn_1$/C-R catalyst synthesized with an initial Pt/Sn precursor ratio at 3:1, while the bulk Pt/Sn ratio was determined to be 10:1 by ICP-OES (Table 1). The XPS spectra of activated carbon support and 2.0%Pt/C-R are presented in Fig. S6 and S7. The assignment of peaks is similar as for 2.0%$Pt_9Sn_1$/C-R nanocatalyst. It is noted that the relative intensity of O 1s peak at 530.7 is greater for 2.0%$Pt_9Sn_1$/C-R than those of 2.0%Pt/C-R and activated carbon support, suggesting that the surface of 2.0%$Pt_9Sn_1$/C-R nanocatalyst is covered with SnO species.

### 3.2. Glycerol oxidation

The prepared PtSn/C nanocatalysts were investigated for glycerol oxidation with purified oxygen as the oxidant. Prior the oxidation reaction, the as-synthesized PtSn/C nanocatalyst was reduced in hydrogen to activate the catalyst. The effect of reduction temperature was studied with 0.5%PtSn/C-R nanocatalyst and the results are displayed in Fig. S8. With the as-synthesized 0.5%$Pt_9Sn_1$/C, 35.7% of glycerol is oxidized at a reaction time of 2 h. The conversion of glycerol is increased to 42.1 and 49.1% by reducing the as-synthesized 0.5%$Pt_9Sn_1$/C nanocatalyst at 200 and 300 °C, respectively. The activity of 0.5%$Pt_9Sn_1$/C-R nanocatalyst remains similar by further increasing the reduction temperature to 500 °C. Thus most of the catalysts were reduced at 300 °C before being used for glycerol oxidation. To study the effect of catalyst loading, 50 mg of 0.5–2.0%$Pt_9Sn_1$/C-R nanocatalysts were used for the reaction. As shown in Fig. 5a and Table 2, the conversion of glycerol was measured to be 14.0% for 0.5%$Pt_9Sn_1$/C-R at reaction time of 2 h. The glycerol conversion is further increased to 25.1%, 33.5%, and 43.1% by increasing Pt loading to 1.0%, 1.5% and 2.0%, respectively. Without modification by Sn, the supported Pt nanocatalyst (2%Pt/C-R) is less active with 29.8% of glycerol converted at 2 h under the same reaction condition. The turn over frequency (TOF) based on total Pt loading was calculated to be 215 and 149 $h^{-1}$ for 2.0%$Pt_9Sn_1$/C-R and 2%Pt/C-R nanocatalysts, respectively. As the catalyst activity could be easily affected by the particle size and exposed surface sites, TEM and CO chemisorption were further carried out to determine the particle size and dispersion of Pt metal. As shown in Table 1, Fig. S9 and S10, the average particle sizes of Pt and $Pt_9Sn_1$ nanoparticles are similar at 1.6 and 1.8 nm, respectively. However, the dispersion of Pt metal was determined to be 52.9%, 22.9 and 0.7% for 2%Pt/C-R, 2.0%$Pt_9Sn_1$/C-R and 2.0%$Pt_{0.8}Sn_1$/C-R nanocatalysts, respectively. The dispersion values could be used to estimate the particle size as 1.7, 3.9, and 128 nm, based on the reported formula [35]. For 2%Pt/C-R catalyst, the size of Pt nanoparticles determined by CO chemisorption and TEM analysis correlates well with each other. It suggests that the surface of Pt is quite clean and with negligible amount of any adsorbed glycolate from the synthesis solution [36]. On the other hand, the discrepancy between PtSn size determined from CO chemisorption and TEM analysis suggests that the Pt surface is covered with SnO species, particularly for 2.0%$Pt_{0.8}Sn_1$/C-R nanocatalysts. The $TOF_{surface}$ based on surface Pt atoms was calculated to be 938 $h^{-1}$ for 2.0%$Pt_9Sn_1$/C-R, which is three times as high as that of 2%Pt/C-R nanocatalysts (281 $h^{-1}$). It is to be noted that the supported $SnO_2$/C is totally inactive for glycerol oxidation. It was reported that both alpha and beta hydrogen abstraction could contribute to the rate determining step[37]. Noble metals are generally believed to be responsible for deprotonation of beta hydrogen. Thus SnO could assist in the first step abstraction of alpha hydrogen through its surface oxygen. Furthermore, it was reported that coordinatively unsaturated iron oxide on Pt nanoparticle surface assisted in activation of oxygen molecules and lowered the activation energy for CO oxidation at

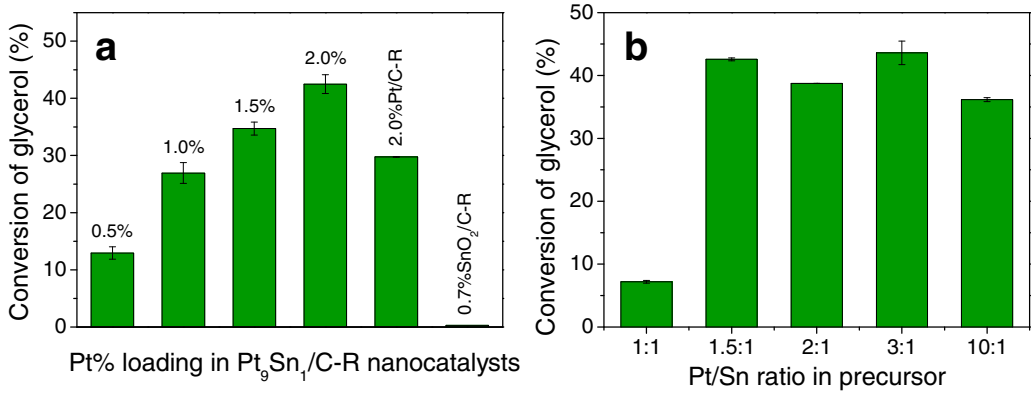


**Fig. 5.** Conversion of glycerol with (a) $Pt_9Sn_1$/C-R nanocatalysts with 0.5–2.0% of Pt loading, 2.0%Pt/C-R, and 0.7%$SnO_2$/C-R nanocatalysts; (b) 2%PtSn/C-R nanocatalysts prepared with various Pt/Sn precursor ratio. Reaction conditions: glycerol (5 mmol), $H_2O$ (10 mL), catalyst (50 mg), oxygen flow (15 mL/min), 60 °C.

**Table 2**
Glycerol oxidation with PtSn/C-R catalysts.[a]

| Catalyst | Conv. (%)[b] | Sel. (%)[c] | | | | | | TOF ($h^{-1}$)[d] |
|---|---|---|---|---|---|---|---|---|
| | | Glyceric acid | Glyceraldehyde | Dihydroxyacetone | Tatronic acid | Hydroxypyruvic acid | Glycolic acid | |
| 0.5%$Pt_9Sn_1$/C-R | 14.0 | 43.9 | 38.2 | 9.8 | 0.7 | 4.5 | 0 | 280 |
| 1.0%$Pt_9Sn_1$/C-R | 25.1 | 43.4 | 39.6 | 12.4 | 0.5 | 7.1 | 1.9 | 251 |
| 1.5%$Pt_9Sn_1$/C-R | 33.5 | 44.5 | 33.1 | 11.9 | 0.6 | 8.5 | 2.0 | 223 |
| 2.0%$Pt_9Sn_1$/C-R | 43.1 | 46.0 | 23.9 | 12.1 | 0.6 | 10.8 | 2.4 | 215 (938)[e] |
| 2.0%$Pt_9Sn_1$/C-R[f] | 91.1 | 55.4 | 1.1 | 7.2 | 1.0 | 19.0 | 8.0 | 113 |
| 2.0%PtSn(10:1)/C-R | 36.3 | 51.8 | 26.3 | 11.8 | 0.7 | 11.4 | 2.9 | 181 |
| 2.0%PtSn(2:1)/C-R | 38.7 | 47.8 | 26.8 | 13.6 | 0.6 | 12.2 | 2.5 | 193 |
| 2.0%$Pt_{0.8}Sn_1$/C-R | 7.3 | 26.3 | 56.4 | 9.9 | 0 | 0 | 0 | 36.5 |
| 2.0%Pt/C-R | 29.8 | 56.9 | 20.7 | 10.0 | 0.6 | 10.3 | 2.7 | 149 (281)[e] |
| 0.7%$SnO_2$/C-R[g] | 0 | – | – | – | | – | – | – |
| 0.5%PtAu(3:1)/C-R[g] | 36.6 | 54.7 | 12.1 | 11.9 | 0.3 | 5.6 | 1.8 | 183 |

[a] Reaction conditions: glycerol (5 mmol), $H_2O$ (10 mL), catalyst (50 mg), glycerol/metal = 1000, oxygen flow (15 mL/min), 60 °C.
[b] Conversion of glycerol was measured at reaction time of 2 h.
[c] Selectivity was defined as mole of product molecules formed over mole of glycerol molecules converted at reaction time of 2 h.
[d] TOF was defined as mole of glycerol molecules converted per mole of total Pt atoms per hour at reaction time of 2 h.
[e] TOF was calculated as mole of glycerol molecules converted per mole of surface Pt atoms (determined from CO chemisorption) per hour at reaction time of 2 h.
[f] Catalyst (100 mg), reaction time of 8 h.
[g] Catalyst (200 mg).

room temperature [38]. For PtSn/C nanocatalyst, the SnO species on Pt nanoparticle surface could function similarly to activate oxygen molecules. The surface adsorbed oxygen atom could function as weak base for abstraction of alpha proton and form surface hydroxyl group, which could bind with surface H atoms to form water and released from catalyst surface. Simultaneously, Pt could abstract the beta hydrogen to produce glyceraldehyde or dihydroxyacetone.

The mole ratio of chloroplatinic acid ($H_2PtCl_6$) and tin chloride ($SnCl_2$) precursors used in the synthesis was adjusted from 10:1 to 1:1 in order to fine tune the loading of Sn in the PtSn nanoparticles. Fig. 5b and Table 1 show that the conversion of glycerol remains similar at 36.3–43.1% for $H_2PtCl_6/SnCl_2$ ratio in the range of 10:1–1.5:1. By further reducing the $H_2PtCl_6/SnCl_2$ ratio to 1:1, the activity of the resultant catalyst (2.0%$Pt_{0.8}Sn_1$/C-R) drops dramatically to 7.3% only at the reaction time of 2 h. The 2.0%$Pt_{0.8}Sn_1$/C-R nanocatalyst was further characterized by XPS technique (Fig. 6). Two peaks at 71.4 and 72.6 eV deconvoluted from Pt $4f_{5/2}$ peak are attributed to Pt at 0 and +2 states respectively as discussed previously. The $Pt^0/Pt^{2+}$ ratio was calculated to be 4, which is higher than that in 2.0%$Pt_9Sn_1$/C-R catalyst ($Pt^0/Pt^{2+}$ = 2.7). The Sn element is partially oxidized with an oxidation state of +2, similar as that in 2.0%$Pt_9Sn_1$/C-R nanocatalyst. Thus the oxidation states of Pt and Sn are not the cause for low activity with 2.0%$Pt_{0.8}Sn_1$/C-R nanocat-

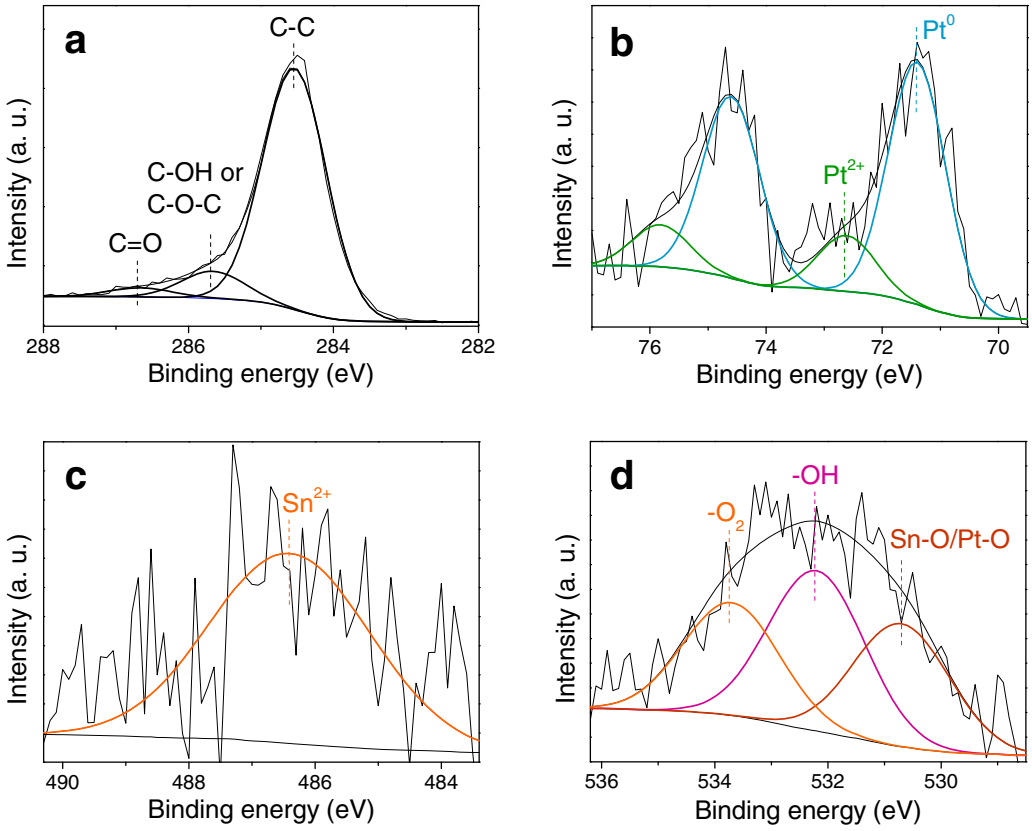


**Fig. 6.** XPS spectra of (a) C 1s, (b) Pt 4f, (c) Sn 3d, and (d) O 1s of 2%$Pt_{0.8}Sn_1$/C-R nanocatalyst.

alyst. On the other hand, the surface Pt/Sn ratio was calculated to be 9 and 0.8 for 2.0%$Pt_9Sn_1$/C-R and 2.0%$Pt_{0.8}Sn_1$/C-R respectively. In fact, the dispersion of Pt was determined to be only 0.7% for 2.0%$Pt_{0.8}Sn_1$/C-R, indicating SnO species have a high surface coverage on $Pt_{0.8}Sn_1$ nanoparticles, and may block the active sites of Pt metal. As mentioned earlier, the supported $SnO_2$ alone is totally inactive for oxidation of glycerol. It suggests that a balance between surface Pt and SnO species is critical for higher activity of glycerol oxidation, as SnO may assist in deprotonation of hydroxyl group and Pt is responsible for abstraction of beta hydrogen from the adsorbed glycerol [16,37]. Furthermore, the average particle size of $Pt_{0.8}Sn_1$ nanoparticles is around 3.2 nm (Fig. S11) which is bigger than those of 2.0%$Pt_9Sn_1$/C-R and 2.0%Pt/C-R nanocatalysts. This can also be one of the reasons for its lower activity.

### 3.3. *Time on course study of 2%$Pt_9Sn_1$/C-R and 2%Pt/C-R nanocatalysts and stability test*

The time on course experiments were carried out for 2%$Pt_9Sn_1$/C-R and 2%Pt/C-R nanocatalysts as shown in Fig. 7. Within 0.5 h, 39.5% and 24.2 % of glycerol is oxidized with 2%$Pt_9Sn_1$/C-R and 2%Pt/C-R catalysts respectively. The conversion is increased to 71.9% at 2 h, and further increased to 91.1% at 8 h for 2%$Pt_9Sn_1$/C-R nanocatalyst (Fig. 7 and Table 2). The glycerol conversion at 8 h is 69.3% for 2%Pt/C-R nanocatalyst. The oxidation of glycerol leads to various products such as glyceric acid, dihydroxyacetone, glyceraldehyde, tatronic acid, hydroxypyruvic acid, and gluconic acid, depending on the degree of oxidation. The selectivity of glyceraldehyde is initially increased to the maximum of 28.1 and 22.1% at 0.5 h, and then gradually decreased to 4.1 and 1.1% for 2%Pt/C-R and 2%$Pt_9Sn_1$/C-R nanocatalysts, respectively (Fig. S12). It is well known that aldehydes could be easily oxidized to respective acids. Thus, the selectivity of glyceric acid is increased steadily to 68.0 and 55.4% for 2%Pt/C-R and 2%$Pt_9Sn_1$/C-R nanocatalysts at reaction time of 8 h. The selectivity of glyceric acid is in the range of 43.4–55.4% for PtSn/C-R nanocatalysts (Table 2). Particularly, 91.1% of glycerol is oxidized with 55.4% selectivity of glyceric acid, resulted in 50.4% yield of glyceric acid (Table 2). As the activity of 2%$Pt_9Sn_1$/C-R is higher comparing to that of 2%Pt/C-R nanocatalyst, more of the formed glyceric acid could further be oxidized to hydroxypyruvic acid for 2%$Pt_9Sn_1$/C-R. In fact, the selectivity of hydroxypyruvic acid is 14.3 and 19.0% at reaction time of 8 h for 2%Pt/C-R and 2%$Pt_9Sn_1$/C-R nanocatalysts, respectively (Fig. S12). It was noted that PtAu nanocatalysts supported on MgO or layered double hydroxide supports were reported to be very active for glycerol oxidation [22,24]. In the present work, PtAu

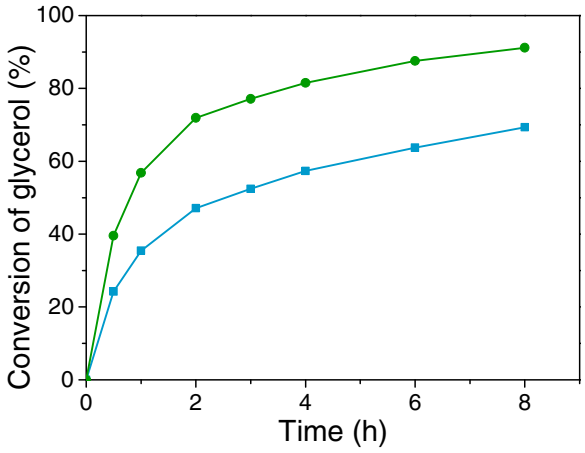


**Fig. 7.** Time on course study of glycerol oxidation with 2%Pt/C-R (blue square) and 2%$Pt_9Sn_1$/C-R (green sphere) nanocatalysts. Reaction conditions: glycerol (5 mmol), $H_2O$ (10 mL), catalyst (100 mg), oxygen flow (15 mL/min), 60 °C. (For interpretation of the references to color in this figure legend, the reader is referred to the web version of this article.)

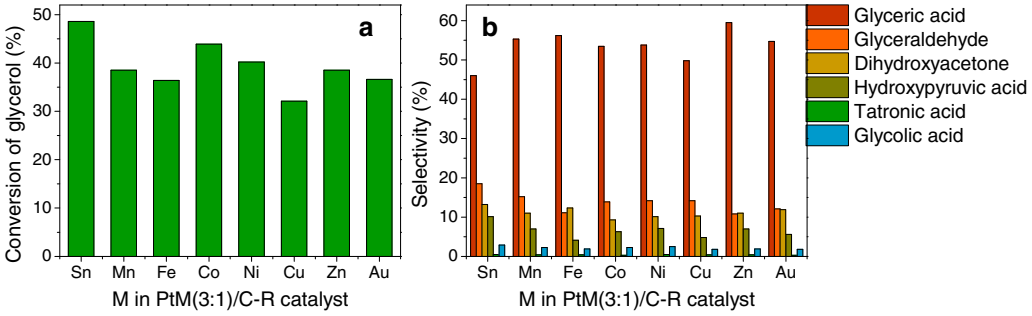


**Fig. 8.** (a) Conversion and (b) selectivity of glycerol oxidation with PtM(3:1)/C-R catalysts (3:1 is the ratio of metal precursors). Reaction conditions: glycerol (5 mmol), $H_2O$ (10 mL), catalyst (200 mg), oxygen flow (15 mL/min), 60 °C. Conversion of glycerol was measured at reaction time of 2 h. Selectivity was defined as mole of product molecules formed over mole of glycerol molecules converted at reaction time of 2 h.

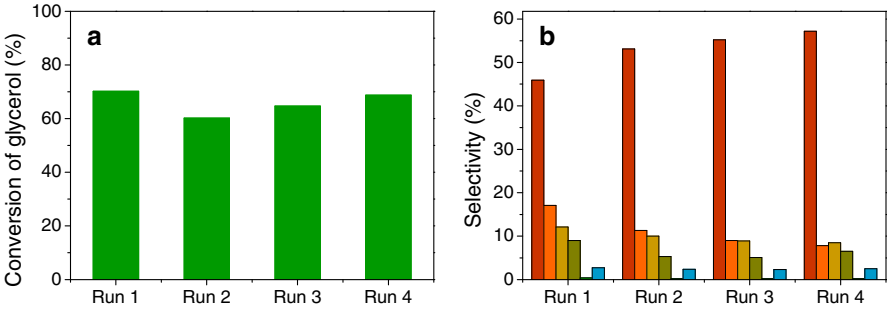


**Fig. 9.** Catalytic stability of 0.5%$Pt_9Sn_1$/C-R was presented with (a) conversion of glycerol and (b) selectivity of oxidation products. Reaction conditions: glycerol (5 mmol), $H_2O$ (10 mL), catalyst (200 mg), oxygen flow (15 mL/min), 60 °C. Conversion of glycerol was measured at reaction time of 6 h. Selectivity was defined as mole of product molecules formed over mole of glycerol molecules converted at reaction time of 2 h.

nanocatalysts were prepared and investigated for glycerol oxidation. The turnover frequency at 2 h was found to be 183 $h^{-1}$ for 0.5%PtAu(3:1)/C-R nanocatalyst. In the case of 0.5%$Pt_9Sn_1$/C-R nanocatalyst, the TOF was calculated to be 280 $h^{-1}$, which is 53% higher than that of 0.5%PtAu/C-R nanocatalyst. Other transition metals (i.e., Mn, Fe, Co, Ni, Cu, and Zn) modified Pt nanocatalysts were prepared similarly using the ethylene glycol assisted reduction method. The prepared nanocatalysts were investigated for glycerol oxidation as well. As shown in Fig. 8, the $Pt_9Sn_1$/C-R nanocatalyst was the most active one for glycerol oxidation under the same reaction conditions.

Finally, the stability of the prepared $Pt_9Sn_1$/C-R nanocatalyst was tested by recycling the used 0.5%$Pt_9Sn_1$/C-R nanocatalyst for 4 runs. As shown in Fig. 9, the $Pt_9Sn_1$/C-R nanocatalyst is very stable with 68.7% conversion of glycerol at the 4th run compared to 70.2% conversion at the initial run. It is to be noted that to restore the initial activity, the recycled catalyst was further treated at 400 °C in $H_2$. It is possibly because that some oxidation products (i.e., ketones) are adsorbed on the catalyst surface [17]. Thus thermal treatment at 400 °C in $H_2$ was carried out to ensure the removal of any adsorbed oxidation products.

## 4. Conclusions

In summary, a range of platinum based nanocatalysts have been prepared with a facile ethylene glycol assisted reduction method. The as-synthesized PtM nanoparticles can be easily immobilized onto the activated carbon support for glycerol oxidation. The carbon support was chosen due to its inertness in acidic reaction solution. The prepared nanocatalysts were thermally treated in hydrogen atmosphere to activate PtM nanocatalysts. Among the various nanocatalysts prepared, $Pt_9Sn_1$/C-R nanocatalyst is the most active for oxidation of glycerol. With 2%$Pt_9Sn_1$/C-R nanocatalyst, a high $TOF_{total}$ of 215 $h^{-1}$ and $TOF_{surface}$ of 938 $h^{-1}$ are attained at reaction time of 2 h at 60 °C. By reducing the loading of $Pt_9Sn_1$ to 0.5%, the $TOF_{total}$ is increased to 280 $h^{-1}$, which is 53% higher than that of 0.5%PtAu/C-R nanocatalyst. With prolonged reaction time of 8 h, 91% of glycerol was oxidized with 50% of glyceric acid yield. Compared with the monometallic 2%Pt/C-R nanocatalyst, the activity (based on surface Pt atoms) of 2%$Pt_9Sn_1$/C-R is two times higher with the addition of Sn. The function of surface SnO species is believed to assist in abstracting proton and/or activation of adsorbed oxygen, leading to lowered overall activation energy for glycerol oxidation. In addition to the high activity for glycerol oxidation, the prepared $Pt_9Sn_1$/C-R has been demonstrated to be very robust by regeneration of the spent catalyst for 3 times without any substantial loss of activity and selectivity.

## Acknowledgement

The authors gratefully acknowledge the financial support provided by Knowledge Built Grant from ExxonMobil Research and Engineering (EMRE) Company, and the Start-Up grant provided by Nanyang Technological University. The authors are also grateful to insightful discussions with Dr. Y. Du from EMRE, and to Mr. J. W. Zheng from Xiamen University for CO chemisorption analysis.

## Appendix A. Supplementary data

Supplementary data associated with this article can be found, in the online version, at http://dx.doi.org/10.1016/j.apcatb.2015.06.007

## References

[1] J.J. Bozell, G.R. Petersen, Green Chem. 12 (2010) 539.
[2] B. Katryniok, H. Kimura, E. Skrzyńska, J.-S. Girardon, P. Fongarland, M. Capron, R. Ducoulombier, N. Mimura, S. Paul, F. Dumeignil, Green Chem. 13 (2011) 1960.
[3] C.H. Zhou, J.N. Beltramini, Y.X. Fan, G.Q. Lu, Chem. Soc. Rev. 37 (2008) 527.
[4] M. Pagliaro, R. Ciriminna, H. Kimura, M. Rossi, C. Della Pina, Angew. Chem. Int. Ed. 46 (2007) 4434.
[5] D. Wang, A. Villa, D.S. Su, L. Prati, R. Schlögl, Chemcatchem 5 (2013) 2717.
[6] W.B. Hu, D. Knight, B. Lowry, A. Varma, Ind. Eng. Chem. Res. 49 (2010) 10876.
[7] F. Porta, L. Prati, J. Catal. 224 (2004) 397.
[8] H. Kimura, K. Tsuto, T. Wakisaka, Y. Kazumi, Y. Inaya, Appl. Catal. A 96 (1993) 217.
[9] C.L. Xu, Y.Q. Du, C. Li, J. Yang, G. Yang, Appl. Catal. B 164 (2015) 334.
[10] J.L. Xu, Y.F. Zhao, H.J. Xu, H.Y. Zhang, B. Yu, L.D. Hao, Z.M. Liu, Appl. Catal. B 154–155 (2014) 267.
[11] E.G. Rodrigues, M.F.R. Pereira, J.J.M. Órfão, Appl. Catal. B 115–116 (2012) 1.
[12] S. Demirel, K. Lehnert, M. Lucas, P. Claus, Appl. Catal. B 70 (2007) 637.
[13] R. Garcia, M. Besson, P. Gallezot, Appl. Catal. A 127 (1995) 165.
[14] S. Carrettin, P. McMorn, P. Johnston, K. Griffin, G.J. Hutchings, Chem. Commun. (2002) 696.
[15] S. Demirel-Gülen, M. Lucas, P. Claus, Catal. Today 102–103 (2005) 166.
[16] Y.K. Kwon, S.C.S. Lai, P. Rodriguez, M.T.M. Koper, J. Am. Chem. Soc. 133 (2011) 6914.
[17] S.A. Kondrat, P.J. Miedziak, M. Douthwaite, G.L. Brett, T.E. Davies, D.J. Morgan, J.K. Edwards, D.W. Knight, C.J. Kiely, S.H. Taylor, G.J. Hutchings, ChemSusChem 7 (2014) 1326.
[18] D. Liang, J. Gao, H. Sun, P. Chen, Z.Y. Hou, X.M. Zheng, Appl. Catal. B 106 (2011) 423.
[19] D. Liang, J. Gao, J.H. Wang, P. Chen, Y.F. Wei, Z.Y. Hou, Catal. Commun. 12 (2011) 1059.
[20] A. Villa, G.M. Veith, L. Prati, Angew. Chem. Int. Ed. 49 (2010) 4499.
[21] M. Kapkowski, P. Bartczak, M. Korzec, R. Sitko, J. Szade, K. Balin, J. Lelątko, J. Polanski, J. Catal. 319 (2014) 110.
[22] D. Tongsakul, S. Nishimura, K. Ebitani, ACS Catal. 3 (2013) 2199.
[23] D. Tongsakul, S. Nishimura, C. Thammacharoen, S. Ekgasit, K. Ebitani, Ind. Eng. Chem. Res. 51 (2012) 16182.
[24] G.L. Brett, Q. He, C. Hammond, P.J. Miedziak, N. Dimitratos, M. Sankar, A.A. Herzing, M. Conte, J.A. Lopez-Sanchez, C.J. Kiely, D.W. Knight, S.H. Taylor, G.J. Hutchings, Angew. Chem. Int. Ed. 50 (2011) 1.
[25] S. Hirasawa, H. Watanabe, T. Kizuka, Y. Nakagawa, K. Tomishige, J. Catal. 300 (2013) 205.
[26] R.F. Nie, D. Liang, L. Shen, J. Gao, P. Chen, Z.Y. Hou, Appl. Catal. B 127 (2012) 212.
[27] W.B. Hu, B. Lowry, A. Varma, Appl. Catal. B 106 (2011) 123.
[28] Q. Wang, G.Q. Sun, L.H. Jiang, Q. Xin, S.G. Sun, Y.X. Jiang, S.P. Chen, Z. Jusys, R.J. Behm, Phys. Chem. Chem. Phys. 9 (2007) 2686.
[29] W.J. Zhou, Z.H. Zhou, S.Q. Song, W.Z. Li, G.Q. Sun, P. Tsiakaras, Q. Xin, Appl. Catal. B 46 (2003) 273.
[30] Y. Wang, J.W. Ren, K. Deng, L.L. Gui, Y.Q. Tang, Chem. Mater. 12 (2000) 1622.
[31] C. Bock, C. Paquet, M. Couillard, G.A. Botton, B.R. MacDougall, J. Am. Chem. Soc. 126 (2004) 8028.
[32] J. Dou, H.C. Zeng, J. Phys. Chem. C 116 (2012) 7767.
[33] W.D. Michalak, J.M. Krier, S. Alayoglu, J.Y. Shin, K.J. An, K. Komvopoulos, Z. Liu, G.A. Somorjai, J. Catal. 312 (2014) 17.
[34] Y.H. Li, J. Xing, Z.J. Chen, Z. Li, F. Tian, L.R. Zheng, H.F. Wang, P. Hu, H.J. Zhao, H.G. Yang, Nat. Commun. 4 (2013) 2500.
[35] M. Turner, V.B. Golovko, O.P.H. Vaughan, P. Abdulkin, A. Berenguer-Murcia, M.S. Tikhov, B.F.G. Johnson, R.M. Lambert, Nature 454 (2008) 981.
[36] C.C. Li, J. Dou, L.W. Chen, J.Y. Lin, H.C. Zeng, ChemCatChem 4 (2012) 1675.
[37] R.M. Painter, D.M. Pearson, R.M. Waymouth, Angew. Chem. Int. Ed. 49 (2010) 9456.
[38] Q. Fu, W.X. Li, Y.X. Yao, H.Y. Liu, H.Y. Su, D. Ma, X.K. Gu, L.M. Chen, Z. Wang, H. Zhang, B. Wang, X.H. Bao, Science 328 (2010) 1141.